BIOCHEMISTRY
including biophysical chemistry & molecular biology

Article

pubs.acs.org/biochemistry

Cystic Fibrosis Transmembrane Conductance Regulator: A Molecular Model Defines the Architecture of the Anion Conduction Path and Locates a "Bottleneck" in the Pore

Yohei Norimatsu,*[,†] Anthony Ivetac,[‡] Christopher Alexander,[†] John Kirkham,[†] Nicolette O'Donnell,[†] David C. Dawson,[†] and Mark S. P. Sansom[‡]

[†]Department of Physiology and Pharmacology, Oregon Health & Science University, Portland, Oregon 97239, United States
[‡]Department of Biochemistry, University of Oxford, South Parks Road, Oxford OX1 3QU, U.K.

Supporting Information

ABSTRACT: We developed molecular models for the cystic fibrosis transmembrane conductance regulator chloride channel based on the prokaryotic ABC transporter, Sav1866. Here we analyze predicted pore geometry and side-chain orientations for TM3, TM6, TM9, and TM12, with particular attention being paid to the location of the rate-limiting barrier for anion conduction. Side-chain orientations assayed by cysteine scanning were found to be from 77 to 90% in accord with model predictions. The predicted geometry of the anion conduction path was defined by a space-filling model of the pore and confirmed by visualizing the distribution of water molecules from a molecular dynamics simulation. The pore shape is that of an asymmetric hourglass, comprising a shallow outward-facing vestibule that tapers rapidly toward a narrow "bottleneck" linking the outer vestibule to a large inner cavity extending toward the cytoplasmic extent of the lipid bilayer. The junction between the outer vestibule and the bottleneck features an outward-facing rim marked by T338 in TM6 and I1131 in TM12, consistent with the observation that cysteines at both of these locations reacted with both channel-permeant and channel-impermeant, thiol-directed reagents. Conversely, cysteines substituted for S341 in TM6 or T1134 in TM12, predicted by the model to lie below the rim of the bottleneck, were found to react exclusively with channel-permeant reagents applied from the extracellular side. The predicted dimensions of the bottleneck are consistent with the demonstrated permeation of Cl^-, pseudohalide anions, water, and urea.

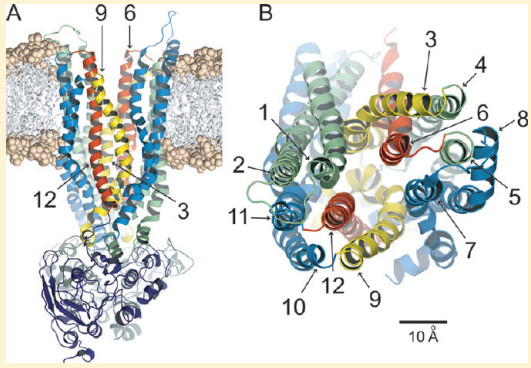

The cystic fibrosis transmembrane conductance regulator (CFTR) is a low-conductance, anion-selective channel that is the product of the cystic fibrosis gene. The properties of the channel have been recently reviewed.[1−3] Three groups recently presented molecular models for the channel based on the crystal structure of the homologous prokaryotic transporter, Sav1866.[4−6] In our modeling, we employed a 5 ns molecular dynamics (MD) simulation to further relax the structure.[6] However, the relatively low level of homology between CFTR and Sav1866, particularly in the membrane-spanning domains (<20%), demands that any model of the CFTR conduction pathway be subjected to extensive experimental validation. In a previous study,[6] we compared the predictions for side-chain orientation in transmembrane segment six (TM6) with the results of experiments in which the reactivity of CFTR constructs bearing cysteine substitutions in TM6 (as defined by hydropathy) was assayed using both channel-permeant and channel-impermeant, thiol-directed reagents applied from the extracellular side of the pore. Channel-permeant, thiol-directed reagents like $[Au(CN)_2]^-$ and $[Ag(CN)_2]^-$ are permeant anions[7] that react with cysteine thiols and deposit a negatively charged substituent by means of a ligand exchange reaction.[8] Permeation of these linear, pseudohalide anions is also consistent with the observation that a cysteine at a single position (e.g., 338) is reactive toward $[Au(CN)_2]^-$ applied to either the extracellular or the cytoplasmic side of the membrane.[8] Larger reagents, like $MTSET^+$ and $MTSES^-$, have been employed in cysteine scanning studies in which reagents were applied from either the extracellular or the intracellular side, and there is general agreement based on the apparent reactivity that these compounds are channel-impermeant.[6,9,10] For most of the TM6 residues tested in our previous study, positions at which substituted cysteines were reactive were predicted by our Sav-based homology model to project into the pore, while those positions at which engineered cysteines were judged to be unreactive were predicted to be occluded by virtue of their orientation and/or juxtaposition with other TMs. In addition, distinct patterns of reactivity for the two classes of reagents suggested a narrowing of the pore on the cytoplasmic side of T338 in TM6. These initial results

Received: December 19, 2011
Revised: February 17, 2012
Published: February 21, 2012

dx.doi.org/10.1021/bi201888a | *Biochemistry* 2012, 51, 2199−2212

suggested that molecular models of CFTR based on Sav1866 would be useful in predicting side-chain orientation and residue location with respect to inner and outer regions of the pore, but the analysis of TM6 did not define the geometry of the CFTR pore or the relation of pore geometry to permeation properties.

Here we present a detailed analysis of the predicted shape of the CFTR pore, in particular the location of a narrow region, or "bottleneck", operationally defined by the differential reactivity of engineered cysteines toward channel-permeant and channel-impermeant, thiol-directed reagents. The bottleneck is predicted to lie just to the cytoplasmic side of T338 in TM6 and I1131 in TM12, residues that mark the experimentally defined cutoff in cysteine reactivity toward channel-impermeant reagents. The effects of amino acid substitutions on the permeation properties make this narrow region a likely candidate for the "selectivity filter" of the CFTR channel. We present cysteine scanning results for TM12, TM3, and TM9, as well as results from additional sites in TM6 that take into account the additional amino acids (over and above those predicted by hydropathy analysis) predicted by modeling the insertion of the CFTR channel into a lipid bilayer. TM6 and TM12 appear to be unique in that they are predicted to line the pore along most of its length. In contrast, TM3 and TM9 are predicted to contribute to the pore lining primarily at the more cytoplasmic end of the pore. Extending the MD simulation to 30 ns predicts the formation of the salt bridge between R352 and D993 envisaged by Cui et al.[11] that was hinted at in our earlier communication.

MATERIALS AND METHODS

Mutagenesis and in Vitro Transcription. Human CFTR cDNA was used in modified pBluescript vectors as described previously.[12,13] In our initial tests of the model,[6] we employed a Cys-less CFTR variant in which all 18 endogenous cysteines were substituted with other amino acids. This construct was a gift from M. Mense and D. Gadsby and was used in their pGEMHE vector.[14] For the experiments described here, however, we employed exclusively the wild-type (wt) CFTR for three reasons. First, with regard to the reactivity of engineered cysteines toward externally applied reagents, our earlier experiments yielded results with the Cys-less CFTR background that were identical to those obtained with the wt background.[6] Second, recently presented evidence suggests that there are functional differences compared to wt CFTR seen with the Cys-less variant.[15,16] Finally, all of our simulations were conducted using the wt CFTR model. The methods used for mutagenesis and in vitro transcription were similar to those reported previously.[12,13] The QuikChange site-directed mutagenesis kit from Agilent Technologies (Santa Clara, CA) was used to generate point mutations in wt or Cys-less CFTR constructs. We mutated individual amino acids in TM3, TM6, TM9, and TM12. Mutations were confirmed by direct DNA sequencing. The CFTR cRNAs for *Xenopus* oocyte injection were synthesized using the mMessage mMachine T7-Ultra in vitro transcription kit from Life Technologies (Carlsbad, CA). After transcription, poly(A) tails were added to the transcripts using *Escherichia coli* poly(A) polymerase as described in the mMessage mMachine T7-Ultra transcription kit.

Cysteine Scanning. The protocol for cysteine scanning, including the control for trace metal contamination, and initial results with TM6 are described in detail by Alexander et al.[6] Briefly, prior to exposure to the thiol-reactive probes employed here, 2-mercaptoethanol (2-ME) or dithiothreitol (DTT) was applied to all oocytes expressing cysteine-substituted CFTR constructs to reverse possible changes in the chemical state of the substituted cysteine due to trace metal contamination as previously described.[17] A ligand exchange reaction between a metal and an engineered cysteine can also be reversed by exposing the oocytes to CN^-, a high-affinity metal ligand in the form of KCN (1 mM). All cysteine-substituted constructs were exposed sequentially to both channel-permeant and channel-impermeant compounds, and changes in conductance were monitored.

Molecular Dynamics Simulation and Analysis. Previously, we built a homology model of CFTR based on the crystal structure of a bacterial homologue, Sav1866, and ran a 5 ns MD simulation using the GROMOS96 force field.[6] In this study, we extended the MD simulation to 30 ns. Snapshots of the CFTR molecule from the simulation were aligned by a least-squares fit using the Cα atoms. The conformational drift of the CFTR channel during the simulation is indicated by the rmsd of Cα atoms from the starting structure. The rmsd increases rapidly in the first nanosecond and then plateaus (reaches equilibrium) before 4 ns. On this basis, frames between 4 and 30 ns were used for analysis of the predicted pore structure.

The pore axis of the CFTR channel was determined with Porewalker[18] using the 5 ns snapshot of CFTR. The shape of the pore in each of the 4−30 ns snapshots (one per nanosecond) of CFTR was examined using HOLLOW.[19] HOLLOW creates a grid of atoms within a user-specified cylinder encompassing the pore of the channel of interest. All the atoms that overlap with the channel protein molecule or lipid molecules of the membrane (if included by the user) are removed, leaving a cast that represents the shape of the pore. The radius of these probing atoms is specified by the user of the program, as is the spacing between the HOLLOW atoms. As the grid spacing is reduced, the casting becomes more accurate, although it increases the computing time. In the study presented here, we used a grid spacing of 1 Å. The casting may be composed of separate components such as intracellular and extracellular vestibules and enclosed cavities. Therefore, we have developed an algorithm to group contiguous HOLLOW atoms and to calculate geometrical properties such as volume, surface area, and cross sectional area. We have also developed an algorithm to determine the largest circle that fits into each cross section of the cast.

To predict pore-lining residues of the CFTR channel, we used PyMol (http://www.pymol.org) to identify atoms located near the casting of the pore interior. A python script was used to automate the identification of residues that lie within 1 Å of the casting. We applied this analysis to residues in each CFTR snapshot and classified them as "pore-lining" if they registered as being within 1 Å of the casting in more than 50% of the MD frames. The automated predictions were also checked by visual inspection of the models.

Oocytes and RNA Injection. *Xenopus laevis* oocytes were extracted and prepared for microinjection using methods previously described in detail.[17,20,21] The follicular membranes were removed by shaking oocytes on a rocking platform (1−2 h) in a Ca^{2+}-free solution containing 82.5 mM NaCl, 2 mM KCl, 1 mM $MgCl_2$, and 5 mM HEPES-Hemi Na (pH 7.5), with 0.2 Wünsch unit/mL of Liberase Blendzyme 3 (Roche Molecular Biochemicals, Indianapolis, IN). Defolliculated oocytes were washed and maintained in a modified Barth's solution containing 88 mM NaCl, 1 mM KCl, 0.82 mM

$MgSO_4$, 0.33 mM $Ca(NO_3)_2$, 0.41 mM $CaCl_2$, 2.4 mM $NaHCO_3$, 10 mM HEPES-Hemi Na, and 250 mg/L Amikacin (pH 7.5). Stage V–VI oocytes were injected with a 50 nL aqueous solution of CFTR cRNA (~4–200 pg/nL) and cRNA encoding the human β_2-adrenergic receptor (~4 pg/nL). CFTR cRNA was diluted to yield 50–200 μS of stimulated conductance. Cys-less variants required 5–10 ng of cRNA per oocyte.

Whole-Cell Recordings. Whole-cell recording methods were similar to those described by Mansoura et al.[22] Individual oocytes were placed in the recording chamber and continuously superfused with Frog Ringer's solution at room temperature (~22 °C). The Ringer's solution contained 98 mM NaCl, 2 mM KCl, 1 mM $MgCl_2$, 1.8 mM $CaCl_2$, and 5 mM HEPES-Hemi Na (pH 7.4). Voltage clamp and data acquisition were performed using the TEVC-200 amplifier (Dagan Corp.) and the pClamp 8 data acquisition program (Axon Instruments, Inc.). The whole-cell $I-V$ plots were constructed by periodically ramping the membrane potential from −120 to 60 mV over 1.8 s approximately once per minute. Between the ramps, oocytes were maintained in the open circuit condition.

Reagents. The experiments described here were conducted using 10 μM isoproterenol (Sigma, St. Louis, MO) and 1 mM 3-isobutyl-1-methylxanthine (IBMX, Sigma) as the stimulating cocktail. Methanethiosulfonate reagents ($MTSET^+$ and $MTSES^-$) were purchased from Toronto Research Chemicals (Toronto, ON). 2-Mercaptoethanol (2-ME), dithiothreitol (DTT), $K[Au(CN)_2]^-$, and $K[Ag(CN)_2]^-$ were obtained from Sigma. KCN was obtained from Fisher Chemicals (Fairlawn, NJ).

RESULTS

Predicted Length of the Transmembrane Segments (TMs). Figure 1A shows the 8 ns CFTR model inserted into a dimyristoylphosphatidylcholine (DMPC) bilayer. A coarse-grained MD simulation was used to obtain an initial estimate of the position of the protein in the bilayer, which was then refined by means of the atomistic MD simulation described in Materials and Methods. Figure 1B shows the outer mouth of the pore viewed from the extracellular side. The TMs are colored to correspond to those illustrated in cross section in Figure 3. It is evident from Figure 1B that TM6 and TM12 are predicted to occupy unique, semisymmetric, pore-lining positions. In contrast, TM3 and TM9 appear to be displaced from the pore interior near the outer mouth of the channel, TM3 lying behind TM6 and TM9 partially behind TM12. These four TMs were the primary focus of this study.

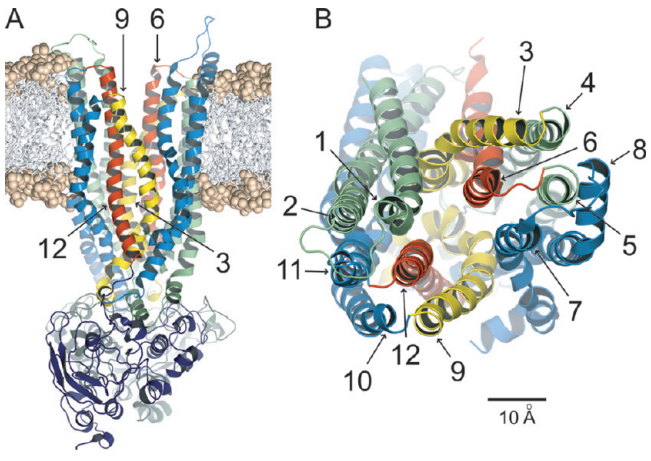

Figure 1. Homology model of CFTR, based on Sav1866. Shown is the 8 ns frame from the MD simulation. Colors: green for TM1, blue for TM2, yellow for TM3 and TM9, and red for TM6 and TM12. (A) Side view of the protein inserted into a DMPC bilayer using an initial coarse-grained MD simulation and subsequent atomistic MD refinement as described in Materials and Methods. Phosphate heads are shown as spheres and hydrocarbon tails as sticks. (B) Top view.

Examination of individual TMs represented in the model revealed that, because of the predicted disposition of the helices in the lipid bilayer, the estimated length of the transmembrane segments differed from that defined by hydropathy.[23] Figure 2 diagrams the changes in the predicted length of the 12 TMs derived from inserting the channel model into the bilayer. These lengths were based on counting residues that were included in the span from one end of the bilayer to the other and did not vary greatly over the 30 ns MD simulation. It can be seen that the models generally predict additional residues that must be considered in any physically realistic definition of the anion conduction pathway. TM6, for example, was defined by hydropathy to comprise 22 residues (G330–T351), whereas insertion of the model into the bilayer predicts a TM6 of 27 residues (T339–L365). Similar, although smaller, differences are apparent in the definition of the extracellular loops. The redefinition of the TMs also relocates an endogenous cysteine (C76) from the cytoplasmic region of membrane-spanning domain 1 (MSD1) into TM1, making a total of five endogenous cysteines in the TMs.

Which TMs Are Predicted To Line the Pore? Figure 3 contains cross sections of the pore taken from the 8 ns MD frame in which each TM is represented by a molecular surface and colored so that it is possible to visualize TMs predicted to contribute to the "pore lining" at various positions along the pore axis. Selected residues in TM6 and TM12, and TM3 and TM9, are indicated for reference. TM6 and TM12 are unique in that they are predicted to line the pore along much of its length as defined here. In contrast, other TMs are predicted to contribute to the pore lining along only a portion of the pore axis. TM3, for example, is predicted to lie behind TM6 in the more extracellular region of the channel but lines the pore along more or less the cytoplasmic half. TM9, although not completely occluded by TM12, is displaced from the pore axis in the extracellular half of the channel and is predicted to move closer to the pore axis in the cytoplasmic half of the channel. TM1 and TM7 are predicted to be pore-lining in the more extracellular portion of the channel but are displaced from the pore axis in the more cytoplasmic region. TM4, TM5, and TM8 are positioned behind TM6 and TM7 in the outer region but move inward to line the large inner cavity in later MD frames. The cross sectional area of the pore interior is colored gray. A space-filling model of the pore interior is considered in more detail below, but the cross sections provide an illustration of the variation in the size and shape of the pore at different axial positions. It is clear, for example, that the area of the irregular pore cross section diminishes as one proceeds down the pore axis from the level of T338 to that of S341 but then expands again before narrowing in the final cross section.

Although the phospholipids comprising the bilayer are not shown in Figure 3, it is apparent that in this MD frame (8 ns) there are gaps in the cross sections at the level of T338 and S341 where lipids are predicted to line the pore. The predicted gaps vary in size from frame to frame but are visible throughout the 30 ns simulation. These gaps derive from the Sav1866

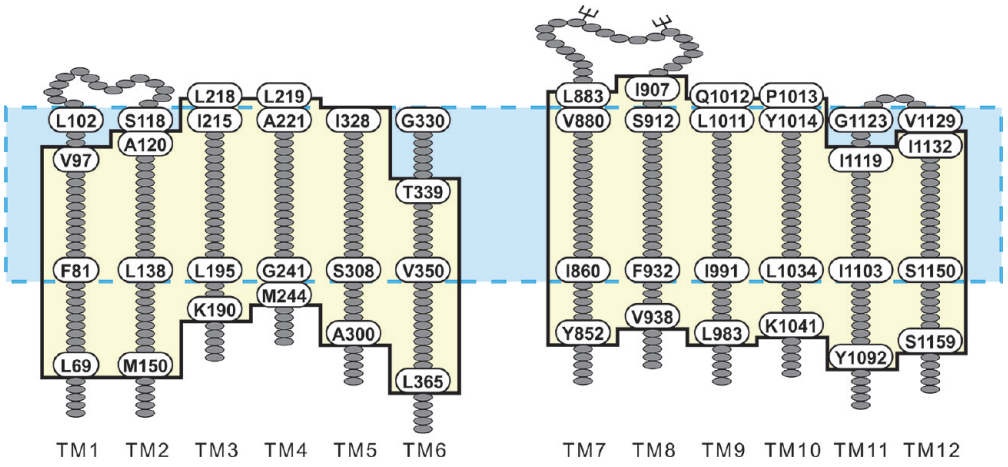

Figure 2. TM segment lengths and boundaries predicted by inserting the model protein into a lipid bilayer differ from those defined by hydropathy analysis. Hydropathy analysis of CFTR yields TM segments 22 amino acids in length,[23] the boundaries of which are illustrated by the blue box with the dashed border. To determine the boundaries of the TMs predicted by the protein bilayer model, 27 MD frames were visually analyzed to determine the amino acids in each TM that were located within the DMPC bilayer. The average boundaries are illustrated by the tan box with the black border. Labeled amino acids define the TM borders predicted by each method.

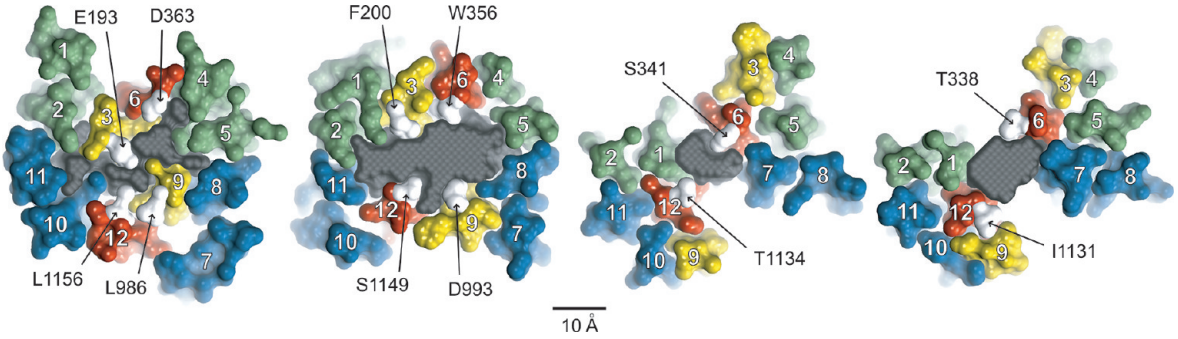

Figure 3. Pore cross sections (8 ns MD frame) at different axial positions. Sections are ordered from extracellular (right-most) to intracellular (left-most). TMs are numbered in white. Individual amino acids from TM3, TM6, TM9, and TM12 are labeled. See Figure 5 for the exact bilayer position of each section. Colors: green for TM1, blue for TM2, yellow for TM3 and TM9, red for TM6 and TM12, and white for labeled residues. The gray area is the cross section of a space-filling model of the pore (casting) defined in more detail in Figures 4 and 5. Labeled amino acids occupy sites where engineered cysteines were found to be reactive toward externally applied, thiol-directed reagents as detailed in the text.

template, captured in the outward-facing conformation, in which the MSDs splay apart forming two "wings".[24,25] Further refinement of the model and more extensive simulation will be required to determine if these gaps are an artifact of the Sav1866 outward-facing template or perhaps openings to the bilayer that appear transiently during the channel gating cycle, and to determine if lipids are predicted to invade the pore. Although not illustrated here, the gaps are most pronounced above the level of the bilayer, in the portion of the channel designated as the outer vestibule. Here approximately 25% of the vestibule boundary is predicted to be open to the external solution, suggesting the possibility that ions might enter the vestibule, not only at the outermost end but also via these side entries. A detailed examination of the electrostatics of this region will be required to ascertain the predicted functional significance of these potential alternate ion entry pathways.

Size and Shape of the Pore. We used HOLLOW[19] to construct a space-filling model, or "casting", of the pore interior that would illustrate how its shape and dimensions vary along the pore axis. HOLLOW creates the casting by filling the volume not occupied by protein or lipid molecules with spheres with a diameter of 2 Å. The general shape prediction was confirmed by visualizing water molecules specified in the MD simulation. In Figure 4, the space-filling model of the pore interior is illustrated in the context of TM6 and TM12 for the

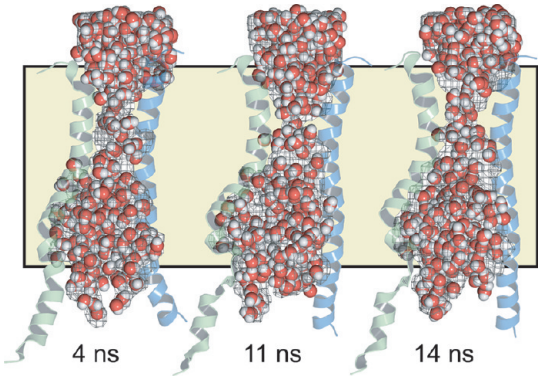

Figure 4. Space-filling model (casting) and distribution of MD waters that make similar predictions for the shape of the CFTR pore. Three representative frames from the MD simulation are shown. Pore casting defined using HOLLOW[19] is represented as a gray mesh. Water molecules are shown as red and white spheres. The position of the lipid bilayer is indicated by the tan shading. TM6 (green) and TM12 (blue) are included to provide a visual reference to the protein.

dx.doi.org/10.1021/bi201888a | *Biochemistry* 2012, 51, 2199–2212

4, 11, and 14 ns MD frames, showing that in each frame the distribution of MD waters confirmed the shape predicted by the space-filling model. For reference, the position of the lipid bilayer is indicated.

Each frame of the MD simulation suggests a well-defined central pore, but as indicated in Figures 3 and 5, the shape and

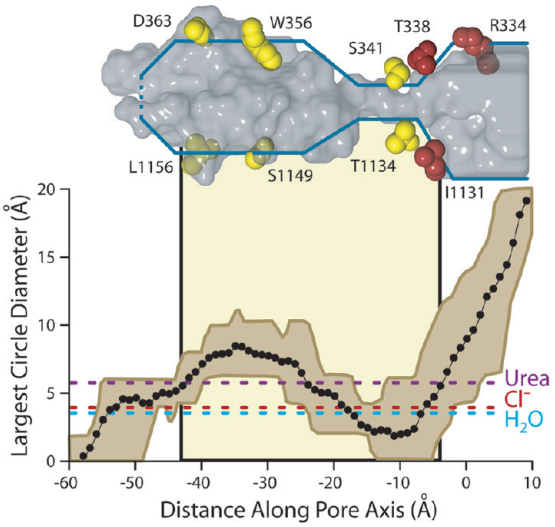

Figure 5. Size of the CFTR pore that varies along the pore axis. Plotted is the mean diameter of the largest circle that can be fitted inside the irregular pore cross sections defined by castings of the 27 MD frames. The brown envelope represents the maximal and minimal values at each axial point. The tan shading in the background indicates the position of the lipid bilayer. Dashed horizontal lines show the diameter of three molecules known to pass through the CFTR pore: urea, chloride, and water (see the text for more details). A representative frame of the casting (16 ns) is shown in gray above the plot. For the orientation, amino acid side chains from TM6 and TM12 are shown and colored on the basis of their reactivity to both channel-permeant and channel-impermeant (red) or only channel-permeant (yellow) reagents. Amino acids shown here are those indicated in the cross sectional slices of Figure 3.

contours vary along the pore axis. Nevertheless, none of the MD frames reveal an opening into the pore from the cytoplasmic side. The pore is roughly hourglass-shaped, comprising an outward-facing vestibule that tapers rapidly toward a narrow bottleneck linking the outer vestibule to a large internal cavity. Mornon et al.[4] called attention to a narrowing of the pore in the vicinity of F337, T338, and S341 but did not delineate its boundaries. The lack of a cytoplasmic opening and the presence of a large internal cavity are both expected in light of the structure of the template for the homology model, Sav1866.[24] The bacterial ABC transporter family, which includes Sav1866, is thought to operate via an alternating access mechanism. In the crystal structures of Dawson and Locher,[24,25] Sav1866 was captured in an outward-facing conformation. In this conformation of Sav1866, a large, polar cavity is visible at the interface of the two membrane-spanning domains, but there is no evidence of a connection of the cavity to the cytoplasm. In the case of CFTR, however, the block of open CFTR channels from the cytosolic side by relatively large organic molecules like glibenclamide led to the postulate of a large, inward-facing cavity such as that predicted here, which would be accessible from the cytoplasmic side when the channel is in the open, anion-conducting state.[26,27]

Pore Dimensions and Permeation. Crossing the narrow region of the pore defined by the models is expected to be the rate-limiting step for the conduction of anions through the CFTR channel. Permeation of a range of halide and pseudohalide anions is well-documented,[7,8,22,28−31] and there is convincing evidence of permeation of water and urea as well.[32] It was of interest, therefore, to estimate pore dimensions and compare them with the sizes of the various permeant species.

Figure 5 contains pore dimensions, estimated by calculating the diameter of the largest circle that could be drawn within the irregular boundary of each cross section, plotted versus the distance along the central pore axis. The diameter plot is aligned with the 16 ns pore casting, illustrating again the irregular and variable predicted cross sectional area of the pore. Marked on the plot for reference are the positions of the lipid bilayer and several residues in TM6 and TM12. The actual area of the irregular cross section traces out a similar geometry and is depicted in Figure S1 of the Supporting Information. The envelope of the diameter plot reflects the range of this parameter within the 27 MD frames. The shape of the pore is generally consistent from 4 to 30 ns, but the simulation predicts considerable flexibility in both the bottleneck and the deeper cytoplasmic cavity. For reference, the diameters of several molecules known to pass through the CFTR pore are shown, including Cl^-, water, and urea.[32] Note that within the range of diameters predicted for the bottleneck by the MD simulation, some values are smaller than that of a chloride ion, suggesting the possibility that this portion of the pore could serve as a gate, or perhaps produce the smaller, subconductance states described by Zhang et al.[33] and Cui et al.[11] In all of the MD frames, the pore appeared to be closed near the cytoplasmic end; that is, the predicted diameter of the most cytoplasmic extent of the anion conduction path was smaller than that of a chloride ion. Other entrances to the pore from the cytoplasmic side were not readily apparent.

Predicting Pore-Lining Residues. A key criterion for judging any molecular model of the CFTR conduction pathway is the accuracy of prediction of amino acid side chains (or backbone elements) that project into the pore and are therefore most likely to experience electrostatic interactions with permeating anions or pore-blocking molecules (see, however, ref 34). To predict the pore-lining side chains for TM3, TM6, TM9, and TM12 in each of the 27 MD frames, we used simple algorithms to identify atoms that lie within 1 Å of the surface of the pore interior as defined by the space-filling model as well as visual inspection. The residues included in this set varied somewhat with each frame of the MD simulation, but there was a large overlap. Model predictions were compared with the results of cysteine scanning experiments in which the reactivity of single cysteines engineered into the CFTR was assayed using both channel-permeant and channel-impermeant, thiol-directed probes applied to the extracellular side of the channel.

Figure 6 summarizes the results of cysteine scanning presented here and in a previous communication[6] derived from experiments employing both channel-permeant and channel-impermeant reagents. Scanning results are tabulated along with consensus predictions for pore-lining residues derived from a survey of 27 MD frames (4−30 ns), as well as the predictions of models developed by Serohijos et al.[5] and Mornon et al.[4] that were also generated using the Sav1866 template but not subjected to MD simulation. Figure S2 of the Supporting Information contains the cysteine reactivity data for

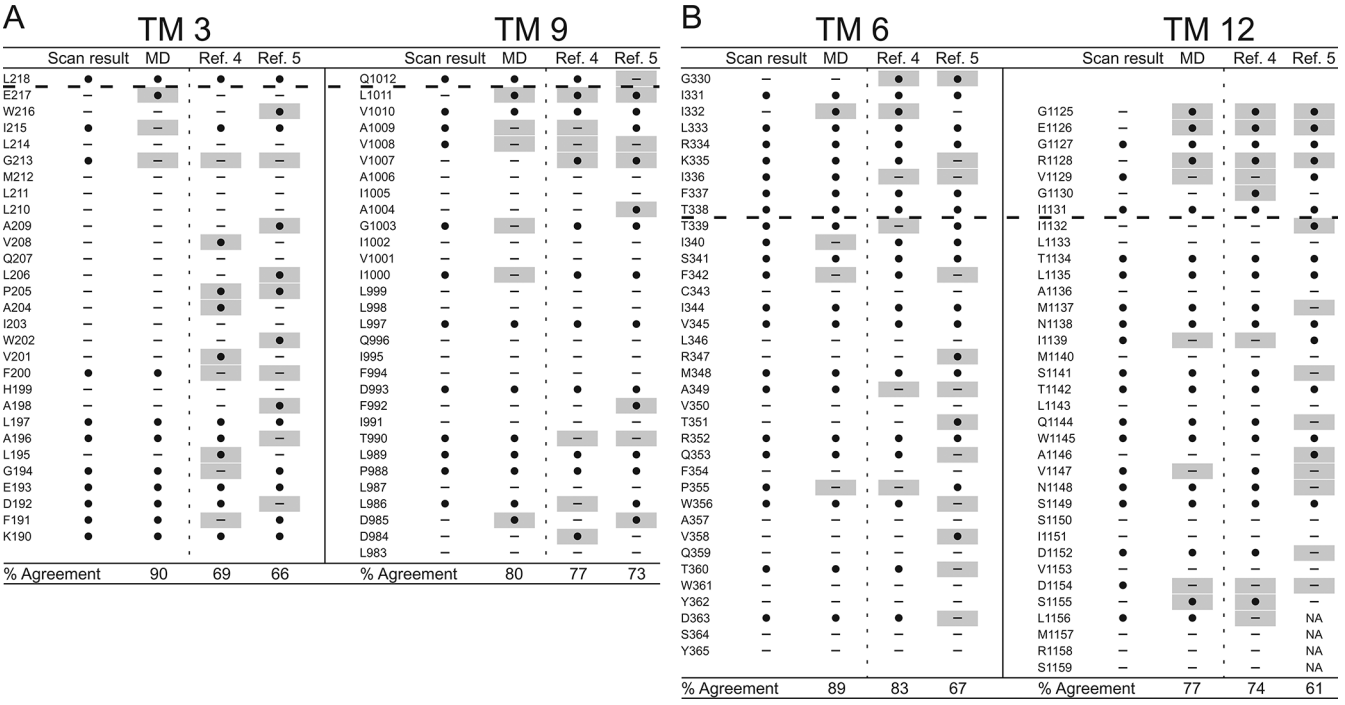

Figure 6. Comparison of results of cysteine scanning using channel-permeant and channel-impermeant probes with predictions of three molecular models of the pore domain of CFTR. (A) TM3 and TM9. (B) TM6 and TM12. The cysteine scanning outcome is labeled Scan result. The MD column contains the consensus predictions of 27 MD frames for pore-lining amino acids (see Materials and Methods for details). Columns labeled Ref. 4 and Ref. 5 contain predictions from Sav-based homology models developed by Mornon et al.[4] and Serohijos et al.[5] (see Materials and Methods for details). (●) Residues where engineered cysteines were reactive by scanning or predicted to be pore-lining. (—) Residues where cysteines were not reactive or predicted to face away from the pore. Sites where scanning data reveal a model prediction to be inaccurate are indicated with a gray box. Amino acids that are not included in a particular model are indicated as NA. Dashed lines indicate the boundaries demarcated by reactivity toward channel-permeant and channel-impermeant reagents as described in the text.

TM3 and TM9 and TM6 and TM12, tabulated as the percent change in CFTR conductance in the presence of the thiol-directed reagent. For TM6, the data include results for the extra residues in the elongated TM6 implicated by inserting the channel into a lipid bilayer (see Figure 2) as well as those originally published by Alexander et al.[6] that were identified on the basis of hydropathy. The tabulated data reveal the expected cutoff in reactivity toward externally applied, channel-impermeant reagents, indicated by the dashed line, and discussed in more detail below. The cutoff occurs just after T338 in TM6, just after I1131 in TM12 and just after L218 in TM3 and Q1012 in TM9. Figure S3 of the Supporting Information contains the results of scanning experiments representative of those from which Figure S2 were derived illustrating the changes in oocyte conductance caused by cysteine modification. It is noteworthy that in several cases (e.g., I1131C) application of $MTSES^-$, which carries a net negative charge, led to an increase in macroscopic conductance. This is likely to be due to an effect on gating, that is, an increase in open probability such as that seen by Bai et al.[35] with $MTSET^+$. Determinations of macroscopic conductance are optimal for revealing the time course of a reaction with an engineered cysteine, but they do not distinguish between effects of the reaction on anion conduction and gating.

It can be seen that the three Sav-based models, as expected, agree on many of the predicted pore-lining residues, but for each of the four TMs considered here, the predictions generated by our MD simulation yielded the best overall agreement with the cysteine scanning results. With the exception of TM3, the predictions derived from the Sav-based model of Mornon et al.[4] are comparable to those derived from the MD simulation. Even in the best cases, like TM3 and TM6 where the scores are ~90%, there are clearly positions at which residues predicted to be pore-lining by the MD simulation do not register in terms of the reactivity of a substituted cysteine and, conversely, sites where cysteines are reactive toward thiol-directed reagents applied from the outside, although the native residue is not predicted to be pore-lining. For example, in TM3 a cysteine substituted at position G213 was reactive toward externally applied, channel-permeant reagents but was predicted by all three models to face away from the pore. Three residues in the outermost region of TM12 (G1125, E1126, and R1128) occupy sites where engineered cysteines are predicted by all three models to be readily accessible to externally applied reagents, but cysteines at these positions did not register as reactive in our assay. In this instance, we cannot eliminate the possibility that reactions did in fact occur but were without functional effect. The differences in model predictions and the discrepancies between predictions and scanning results underline the need for further refinement of the homology models, as well as perhaps a more sophisticated understanding of possible differences in local protein conformation that may be induced by cysteine substitution.

Comparing Cysteine Scanning Results for Pore-Lining Residues. Figure 7 compares our cysteine scans of TM6 and TM12 using externally applied, channel-permeant and channel-impermeant, thiol-directed probes with results reported by two other laboratories. The latter experiments were conducted using inside-out membrane patches, detached from either BHK

dx.doi.org/10.1021/bi201888a | *Biochemistry* 2012, 51, 2199–2212

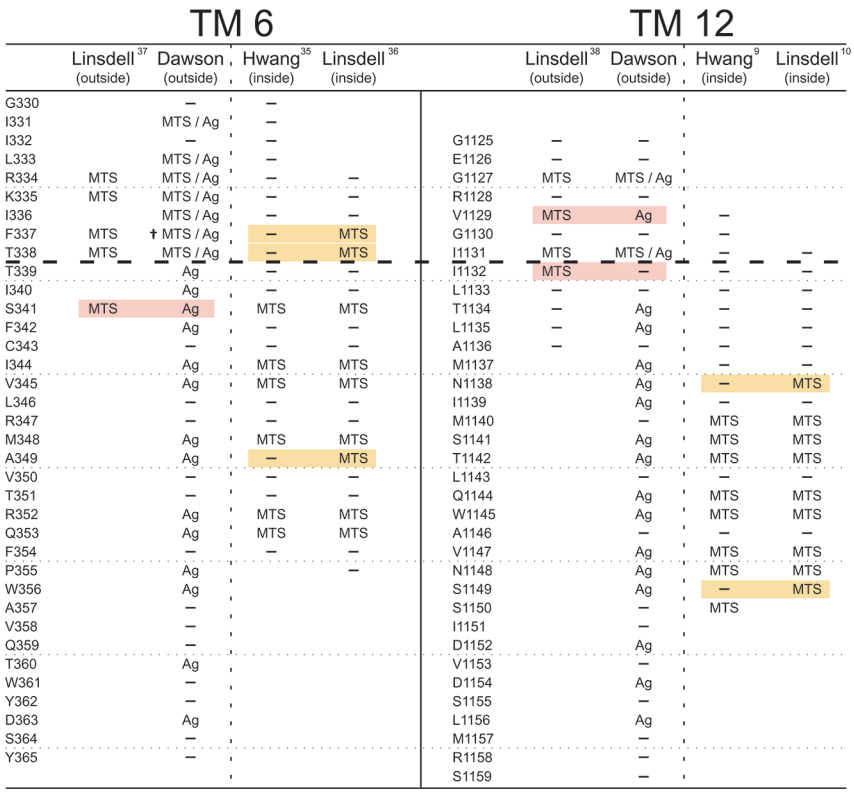

Figure 7. Comparison of cysteine scanning results for TM6 and TM12 presented here with previously published data from two laboratories. Each column collects scanning results obtained by the indicated laboratories using either externally applied or internally applied, thiol-directed reagents as indicated. Positions where MTS reagents and/or $[Ag(CN)_2]^-$ were reported to be reactive with engineered cysteines are labeled accordingly. Positions where no reactivity was reported are labeled with bold dashes. Positions that were not tested are blank. Shading indicates a position where results differ between laboratories. While there is agreement between laboratories for the majority of residues, residues where there is disagreement tend to lie in the region predicted by the model presented here to be the narrowest portion of the pore. The dagger denotes that F337C was previously reported by our group to be unreactive toward $MTSET^+$ and $MTSES^-$. While this result holds for experiments performed at room temperature, we have found that reactivity toward these reagents can be induced by increasing the temperature of the experimental chamber to 37 °C.[62] It should be noted that additional discrepancies exist in the results obtained by different laboratories that are more subtle in nature than the more-or-less binary "reactive–not reactive" paradigm conveyed in this figure. Interested parties are encouraged to consult the relevant cited publications.

cells[10,36–38] or CHO cells.[9,35] Both studies utilized exclusively channel-impermeant probes that were applied to either the cytoplasmic side or the extracellular side of the membrane using two strategies. Reagents could be applied to the cytoplasmic side of detached inside-out patches by adding the compound to the bathing solution.[9,10,35,36] External application of reagents was achieved by detaching patches from cells preincubated in reagent or by including the reagent in the pipet solution.[10,36–38] These methods of external application unfortunately share several serious weaknesses. They do not permit either the extent or the rate of the reaction to be discerned, nor do they generally allow for subsequent exposure of the membrane to other reagents (e.g., reducing agents or metal ligands) that might be used to verify the nature of the presumed reaction and thereby control for artifacts due to trace metal contamination.[6,17]

The dashed line in Figure 7 indicates the boundary between the observed reactivity of substituted cysteines toward channel-permeant and channel-impermeant reagents applied from the extracellular side of the channel detected in this work, as well as a previous study by our lab.[6] Below the line, engineered cysteines were found to react only with channel-permeant reagents. There is significant overlap in the scanning results obtained by the three laboratories, but there are also important discrepancies. These will be considered in detail in Discussion, but we call attention here to the primary difference, namely the position of the bottleneck in the pore empirically defined by the pattern of reactivity toward channel-impermeant reagents like $MTSES^-$. In scanning assays of TM6 and TM12 by Fatehi and Linsdell[37] and Fatehi and Linsdell,[38] cells were preincubated with reagent or reagent was present in the pipet solution so that reactivity was gauged solely on the basis of changes in the shape of the *I*–*V* plot. Their results were interpreted as yielding evidence of reactivity toward externally applied reagents at positions lying cytoplasmic to the cutoff defined here, specifically, positions 341 in TM6 and 1132 in TM12. Scans from the inside conducted by Bai et al.[35] and El Hiani and Linsdell[36] differed in a similar fashion. Whereas Bai et al.[35] reported that residue 341 was the most outward-lying TM6 residue where cysteine reactivity toward cytoplasmically applied reagents was detectable, El Hiani and Linsdell[36] detected reactivity toward cytoplasmically applied MTS compounds at positions 338 and 337 as well. In scans of TM12 from the inside, reactivity was reported by Qian et al.[10] for a cysteine substituted at position 1138, whereas reactivity reported by Bai et al.[9] extended to only position 1140.

Figure 8 depicts the pore-lining residues identified in TM3 and TM9 by cysteine scanning in the context of the molecular

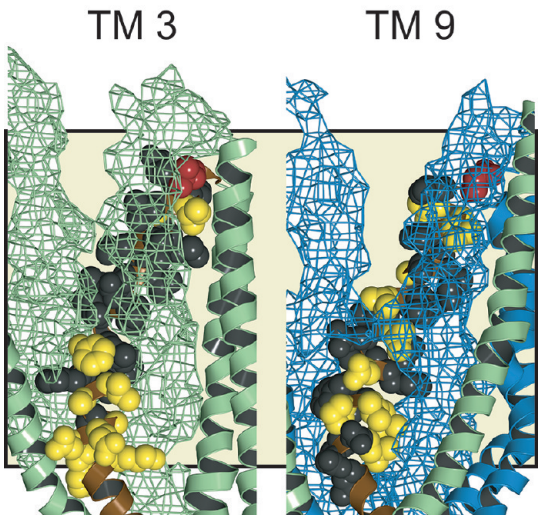

Figure 8. Pore-lining residues defined by cysteine scans of TM3 and TM9. Amino acids examined in this study are indicated in the 8 ns MD frame. Side views are shown, with various TMs removed to reveal the pore-lining face of the TM of interest. TM segments that appear to partially occlude engineered cysteines are represented by a space-filling mesh (green for TM1 and TM6 in the TM3 panel and blue for TM7 and TM12 in the TM9 panel). Residues where cysteines were reactive with both channel-permeant and channel-impermeant reagents are colored red. Those that were reactive exclusively toward channel-permeant reagents are colored yellow. Residues where no reactivity was observed are colored black. TM1 segments are colored green. TM2 segments are colored blue. Tan background shading indicates the position of the lipid bilayer.

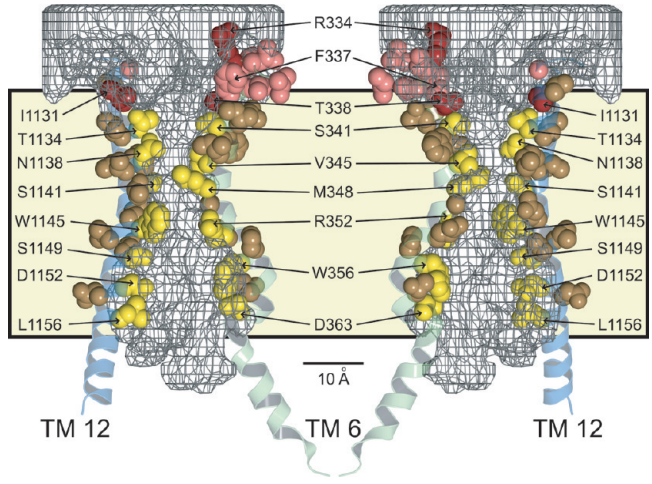

Figure 9. Pore-lining residues predicted by the molecular model and confirmed by cysteine scanning, showing that the cutoff in reactivity of engineered cysteines toward externally applied, channel-impermeant, thiol-directed reagents coincides with the predicted narrowing of the pore. Sites in TM6 (green) and TM12 (blue) are shown in the context of two views (front and back) of the 8 ns MD frame together with the pore casting (gray mesh) and the lipid bilayer (tan shading). Red/pink (dual colors for clarity of visualization) for residues where cysteines were reactive toward both channel-permeant and channel-impermeant reagents. Yellow/brown (dual colors for clarity of visualization) for residues where cysteines were reactive toward only channel-permeant reagents. The cutoff in reactivity toward externally applied, channel-impermeant reagents aligns with a dramatic narrowing of the pore interior.

model for the pore. Residues colored red are those where engineered cysteines reacted with both channel-permeant and channel-impermeant, thiol-directed probes, and as expected, these positions lie in the outermost region of the pore. Those residues colored yellow are positions where engineered cysteines were reactive exclusively toward externally applied, channel-permeant probes. Accordingly, they are positioned deeper in the conduction path. Residues represented in black are sites where substituted cysteines scored as unreactive toward both channel-permeant and channel-impermeant probes. In the case of TM3, the reactivity of engineered cysteines was generally absent in the more extracellular region where engineered cysteines were occluded by TM1 and TM6 as illustrated in Figure 8, in which the two occluding TMs are represented as a mesh surface. In contrast, in the more cytoplasmic portion of TM3, predicted by the model to line the pore, cysteine reactivity toward the channel-permeant probe, $[Ag(CN)_2]^-$, was evident. Cysteines substituted into TM9 are predicted by the model to be partially occluded by TM12 and TM7 near the extracellular end of the pore, and cysteine reactivity was generally absent there.

The Differential Reactivity of Engineered Cysteines Confirms the Predicted Outer Edge of the Bottleneck. A comparison of the modification patterns of cysteines engineered into the principal pore-lining TMs, TM6 and TM12, reveals a distinct and spatially consistent demarcation between reactivity toward externally applied, channel-permeant and channel-impermeant probes (Figures 6B and 9). This boundary lies just to the cytoplasmic side of position 338 in TM6 and position 1131 in TM12. Cysteines at either of these positions reacted with externally applied $MTSET^+$ and $MTSES^-$, as well as $[Ag(CN_2)]^-$, whereas cysteines inserted just below these positions, that is at positions 341 (TM6) and 1134 (TM12), reacted only with the channel-permeant probe, $[Ag(CN_2)]^-$. Figure 9 shows two views ("front" and "back") of selected, pore-lining side chains of TM6 and TM12, confirmed by cysteine scanning, in the context of the space-filling model (casting) of the pore interior. The predicted positions of T338 in TM6 and I1131 in TM12 coincide with the extracellular boundary of the bottleneck, as if they form a portion of an outer lip at the most extracellular end of the narrow portion of the pore. In contrast, S341 (TM6) and T1134 (TM12), where substituted cysteines are reactive only toward channel-permeant probes (externally applied), are predicted to lie below the lip of the bottleneck and within the narrow region of the pore. The distinct cutoff in reactivity toward externally applied thiol probes seen in both TM6 and TM12 is consistent with the notion that neither $MTSET^+$ nor $MTSES^-$ can pass through the pore bottleneck. Figure 9 locates R334 in the water-filled, outer vestibule,[6] consistent with its demonstrated role in providing a positive electrostatic potential in this region of the pore.[13,39,40]

Predictions for TM6−TM12 Cysteine Cross-Linking. As a further test of predicted pore geometry, we measured the predicted distances between the TM6−TM12 cysteine pairs employed by Chen et al.[41] in their study of the efficacy of cross-linking by bismethanethiosulfonate (bisMTS), thiol-directed probes. They employed three probes of varying lengths, 1,5-pentanediyl-bisMTS (M5M), 3,6-dioxaoctane-1,8-diyl-bisMTS (M8M), and 3,6,9,12,15-pentaoxaheptadecane-1,17-diyl-bisMTS (M17M), and tested CFTR constructs containing four different cysteine pairs, C348−C1142, C351−C1142, C351−C1143, and C356−C1145. We derived the predicted distribution of sulfur−sulfur distances for the cysteine pairs in

dx.doi.org/10.1021/bi201888a | *Biochemistry* 2012, 51, 2199−2212

our model by mutating the appropriate residues in PyMol using MD frames from 4 to 30 ns. Figure S4 of the Supporting Information illustrates the positions of the six engineered cysteines in the mutated CFTR. The effective length of the bisMTS probes was estimated using 12 ns MD simulations in explicit water to predict the dynamic distribution of the distance between the two most distal sulfur atoms on the ends of the probe molecule, both of which are mixed disulfides.

Chen et al.[41] observed cross-linking of M348C and T1142C by M5M and M8M but not M17M. Our CFTR models predict both of these residues to be pore-lining, and engineered cysteines at both locations were reactive toward thiol-directed probes employed here and in other studies.[9,10,35,36] The predicted distribution of the C348−C1142 sulfur−sulfur distances overlapped with the predicted dynamic distribution of the inter-sulfur distances for M5M and M8M, consistent with cross-linking results. The distance comparison was also compatible with C348−C1142 cross-linking by M17M, but this was not seen by Chen et al.[41] The lack of experimental cross-linking with M17M may reflect pore dimensions near positions 348 and 1142 where the average diameter is predicted to narrow to ~6 Å. The two ends of M17M are predicted by the MD simulation to come close to each other in free solution, forming a folded structure, theoretically allowing cross-linking of engineered cysteines such as M348C and T1142C. However, this structure does not fit into the narrow part of the pore in the vicinity of the target residues.

Chen et al.[41] observed C351−C1142 cross-linking in M8M and M17M but not M5M. The predicted distribution of sulfur−sulfur distances for C351−C1142 overlapped with the dynamic range of M8M and M17M but not with that of M5M, consistent with the observations of Chen et al.[41] A cysteine at position 351, however, was not reactive toward thiol-directed reagents, externally or internally applied, in three separate studies.[6,35,36] T351 is, however, predicted by the model of Serohijos et al.[5] to be pore-lining, and visual inspection of our model reveals that the orientation of the native side chain is just slightly displaced from a pore-lining position. It may be that in the double-cysteine mutant, which was built on a Cys-less background, the protein conformation was altered so as to render C351 probe-accessible.

Chen et al.[41] did not observe cross-linking of T351C and L1143C with any of the three cross-linking agents. This result is not surprising in view of the fact that a Cys at position 1143 was not reactive toward thiol-directed reagents in this and two other studies,[9,10] nor was it predicted to be pore-lining by any of the three models considered here. Chen et al.[41] observed C356−C1145 cross-linking by M5M, M8M, and M17M, two predicted pore-lining sites where substituted cysteines are reactive toward thiol-directed reagents. The predicted distribution of the C356−C1145 sulfur−sulfur distance did not overlap with the dynamic range of M5M and barely overlapped with that of M8M but coincided with that of M17M. This difference, between the observation of Chen et al.[41] and our prediction, could reflect flexibility in the size of the internal cavity that is not apparent in our model.

Predicted Protein Motion. The 30 ns MD simulation predicts significant motion of the TMs, and the consequences of this motion constitute an important test of the validity of the model. Cui et al.[11] proposed, on the basis of the effects of amino acid substitutions on single-channel conductance and gating kinetics, that R352 in TM6 and D993 in TM9 might form a salt bridge during some portion of the gating cycle and thereby stabilize the conducting state. Both of these residues lie at sites where engineered cysteines were reactive toward externally applied, channel-permeant reagents (Figure 6), indicating that they contribute to the lining of the pore. We reported previously that a 5 ns MD simulation indicated that these side chains appear to move toward each other. Figure 10 compares the predicted, relative positions of the two side chains in the 9 and 19 ns MD frames. It can be seen that at 9 ns the van der Waals radii of the two residues are predicted to overlap, whereas at 19 ns, they are separated by the maximal distance, ~8 Å. The prediction of the MD simulation is consistent, therefore, with the proposal by Cui et al.[11] that the salt bridge forms transiently during the gating cycle.

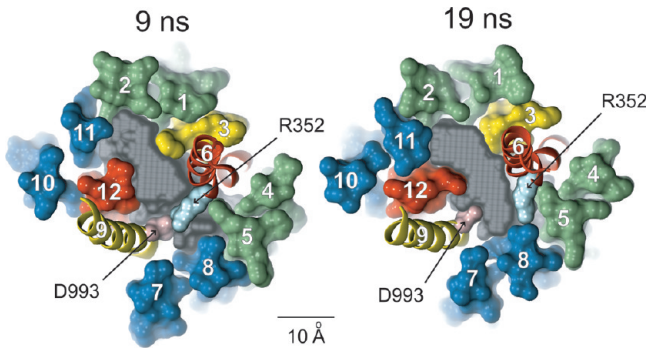

Figure 10. MD simulation predicts the transient formation of a salt bridge between R352 (TM6) and D993 (TM9), as postulated by Cui et al.[11] Shown are cross sections of the 9 and 19 ns MD frames illustrating the relative movement of these two residues. Colors: green for TM1, blue for TM2, yellow for TM3 and TM9, red for TM6 and TM12, gray for casting, light blue for R352, and pink for D993. Both residues occupy sites where engineered cysteines are reactive toward externally applied, channel-permeant, thiol-directed reagents.

DISCUSSION

Size and Shape of the CFTR Pore. The results presented here extend those presented by Alexander et al.[6] regarding the validation of a Sav1866-based homology model for the CFTR pore. In particular, the predicted contributions of TM3, TM6, TM9, and TM12 to the pore were examined and compared to the results obtained using cysteine scanning. TM6 and TM12 are predicted to make important contributions to the lining of the pore along most of its length, a result that is not unexpected in view of the structure of the template protein, Sav1866, as well as the related ABC transporter, P-glycoprotein.[24,25,42,43] Cysteine scanning, taking into account those positions where reactivity is not predicted, resulted in an average of 84% agreement between reactivity and predicted location in the pore. This result suggests that, although not perfect, the model produces a reasonably accurate representation of side-chain orientation that may be further improved by adjustments to the alignment of the CFTR and Sav1866, as well as exploration of other pore conformations.[44] The pore is closed at the cytoplasmic end in all MD frames, and it is possible that the structure of a truly "open pore" would be altered in a way that would improve agreement between predicted and experimentally defined pore-lining residues. Mornon et al.,[44] however, created a CFTR model based on the crystal structure of an inward-facing conformation of MsbA and identified a narrow pathway for anions that would connect the channel with the cytoplasm. Predicted pore-lining residues were, however,

similar to those derived from a Sav1866-based model. TM3 and TM9 are predicted by the Sav-based model to contribute to the pore largely in the more inner-lying regions, a result largely confirmed by cysteine scanning. The functional significance of these residues for conduction and gating remains to be explored.

Pore Architecture and Channel Properties. A set of general features of the CFTR anion conduction path has emerged from an abundance of electrophysiological studies conducted over more than two decades that can be compared to the predictions of the models presented here. The channel is highly selective for anions over cations but relatively nonselective among anions, conducting Cl^-, Br^-, I^-, $[NO_3]^-$, $[SCN]^-$, $[OCN]^-$, $[N(CN)_2]^-$, $[Au(CN)_2]^-$, $[Ag(CN)_2]^-$, and $[C(CN)_3]^-$, anions that range in size (equivalent spherical diameter) from 3.62 Å (Cl^-) to 6.08 Å {$[C(CN)_3]^-$}.[7] Anion selectivity, defined by permeability ratios derived from reversal potential changes or by the ability of substitute anions to bind in the channel and block Cl^- flow, follows a lyotropic series in which anions with the lowest free energy of hydration enter the channel more readily and also bind more tightly.[7,45] The conduction process is reasonably well described by a simple two-barrier, one-well rate theory model[7] that accounts for the energetics of anion conduction, although more complex models have also been proposed.[46−49] The magnitude of channel conductance and the shape of the channel current−voltage relation are highly dependent on the charge associated with R334,[13,40] predicted by the model to lie within the outer vestibule of the pore.[6,39] Blockade of CFTR channels by impermeant, organic blockers has been used to operationally define a large, intracellular vestibule.[26,27,50,51] The CFTR channel exhibits permeability to water and urea.[32] Each of these properties is addressed below in relation to model predictions.

Is the Bottleneck the CFTR Selectivity Filter? To account for the relative anion nonselectivity of CFTR, Smith et al.[7] and Dawson et al.[52] invoked the notion of a "polarizable tunnel" to describe the stabilization of a variety of anions within a CFTR pore that was predicted to lack a highly specialized, anion-coordinating structure like that familiar in potassium channels. The outer vestibule of the molecular model for the CFTR pore tapers rapidly toward a narrow bottleneck, which is an obvious candidate for the polarizable tunnel postulated to be the site of lyotropic selectivity among anions, particularly that defined by anion binding. The bottleneck separates two aqueous vestibules in which anions would be stabilized by water molecules.[52−55] As illustrated in Figure 5, it is easy to imagine that the two barriers and single well of the simple kinetic model for anion conduction reflect a three-step, translocation process by which anions partition from one of the vestibules into the bottleneck, bind transiently therein, and then exit on the other side, leaving the pore via the other vestibule. The MD simulation predicts that water molecules not only are abundant in the outer and inner vestibules but can also inhabit the narrow region of the pore. Entry of an anion into the bottleneck may involve the loss of some, but not all, of the inner sphere waters that coordinate the anion in the vestibules. Larger permeant anions would see a lower barrier to entry into the bottleneck due to their reduced energy of interaction with vestibule waters. Once inside the bottleneck, binding of anions would require that they be at least partially coordinated by side-chain elements, potential candidates being hydrogen bonds with Ser341 in TM6 and Thr1134 in TM12, as well as a possible interaction with nonpolar hydrogens[56,57] and the positive charge on Lys95.[50,51] The tighter binding of the larger anions like $[SCN]^-$, $[Au(CN)_2]^-$, and $[C(CN)_3]^-$ would reflect their reduced energy of hydration as well as perhaps strengthened anion−channel interactions due to increased polarizability.[58]

Anion Selectivity. Previous studies from several laboratories have strongly implicated residues that are predicted to comprise the bottleneck of the pore as contributing to the ability of CFTR to discriminate between anions. McDonough et al.[59] first drew attention to TM6 and TM12 residues that reside within the bottleneck, specifically, S341 (TM6) and T1134 (TM12), as potential contributors to the binding of a channel blocker, diphenylamine-2-carboxylate (DPC). Amino acid substitutions for a residue predicted to inhabit the outer rim of the bottleneck, T338, altered permeability ratios determined from reversal potentials[30] and the anion conductance sequence.[60] McCarty and Zhang[61] conducted a systematic study in which they substituted residues in TM6 with alanine and compared anion permeability and conductance ratios. They concluded that T338 and S341 lay within a region of "strong discrimination" that was likely to be at or near the narrowest part of the pore, presumed to be the selectivity filter. One unifying scenario would envision the side chain of S341 contributing to the stabilization of anions within the bottleneck. Moving from the bottleneck to the outer vestibule would involve a transition state in which the anion could be partially stabilized by a hydrogen bond with the side chain of T338 as it re-entered an essentially aqueous environment. Our molecular model places T338 on the outward-facing rim of the bottleneck, a position that is consistent with the reactivity of a cysteine at this site toward externally applied reagents that is rapid and nonselective.[6,40,62]

Pore Diameter. The notion of "pore diameter" is expected to be a somewhat elusive concept structurally in that properties other than the size and shape of a molecule can determine how well it is accommodated within the anion conduction pathway. Functional studies, based on comparisons of permeation and molecular dimensions, have generally placed the limiting diameter of the CFTR pore somewhere between 5 and 6 Å.[32,63,64] Hasegawa et al.[32] described the cAMP-dependent movement of water and urea through the CFTR channel. The Sav-based homology model predicts that in the 8 ns frame as many as three water molecules, or at least one urea molecule, could occupy the narrowest point in the pore. Hasegawa et al.[32] estimated the permeability ratio, P_{water}/P_{urea}, to be on the order of 1000:1. This is consistent with the estimated pore dimensions illustrated in Figure 5 suggesting that water would pass easily through the pore bottleneck whereas urea would be a tighter fit. Our previous comparison of the permeation of pseudohalide anions indicated conduction of $[C(CN)_3]^-$. Molecular models of the compound suggest the diameter of the smallest cylinder through which $[C(CN)_3]^-$ can squeeze is 7.5 Å, but the molecule is planar and more or less coin-shaped, having a height of only 3.4 Å so that it would fit through a slot-shaped opening such as that predicted by the CFTR molecular model. For example, in the 5 ns MD frame, in which the size of the bottleneck is predicted to be near its maximum, a $[C(CN)_3]^-$ molecule can pass through the bottleneck as can the urea molecule (limiting cylindrical diameter, 5.7 Å; height, 3.4 Å).

Locating the Barrier to the Permeation of $MTSES^-$. Our cysteine reactivity comparisons suggest that $MTSES^-$,

despite its anionic character, cannot pass from the outer vestibule into or through the pore bottleneck and react, for example, with a cysteine substituted at position 341. The limiting cylindrical diameter of the rod-shaped $MTSES^-$ molecule can be estimated from molecular models to be ~6.1 Å, so that the bottleneck dimensions suggested by the molecular model would preclude the permeation of $MTSES^-$. The maximal diameter of the largest circle that could be drawn within the bottleneck region in a range of structures from the MD simulation was predicted to be ~5 Å. The minimal diameter is close to zero, and the bottleneck nearly pinches off in some MD frames. Bai et al.[35] scanned TM6 from the inside using CHO cells transiently transfected with cysteine-substituted constructs and obtained results compatible with the pore geometry proposed here. Reactivity toward cytoplasmically applied $MTSET^+$ and $MTSES^-$ extended only to a Cys at position 341; cysteines at positions 338 and 337 were not reactive toward cytoplasmically applied MTS reagents. Taken together, these results and those of Bai et al.[35] place the functional barrier to externally applied $MTSES^-$ and $MTSET^+$ extracellular to position 341 and cytoplasmic to position 338, implying that thiol reactivity places the most sterically restrictive portion of the pore bottleneck in a very short region comprising approximately one helical turn of TM6 between T338 and S341, a location that is consistent with model predictions.

El Hiani and Linsdell[36] also recently studied the accessibility of cysteines engineered into TM6, using patches detached from BHK cells, but reported reactivity to cytoplasmically applied MTS reagents extending beyond position 341, to positions 338 and 337. This latter result is puzzling in that at the most distal site, position 337, the cationic $MTSET^+$ was deemed reactive whereas the anionic $MTSES^-$ was not. Results of El Hiani and Linsdell[36] for a Cys at position 338 are similarly puzzling. Here, they report that both $MTSET^+$ and $MTSES^-$ were reactive, again requiring a large, cationic reagent to traverse the most narrow portion of an anion-selective pore. Fatehi and Linsdell[37] had previously reported that when the reagents were present on the extracellular side of detached patches, modification of the shape of the $I-V$ plot by extracellular $MTSET^+$ and $MTSES^-$, applied using a preincubation protocol or by including the reagent in the pipet, extended to position 341. Alexander et al.,[6] in contrast, reported a cysteine at this site to be reactive only toward the channel-permeant reagent, $[Ag(CN)_2]^-$, when applied outside the cell. Neither of the channel-impermeant regents, $MTSET^+$ or $MTSES^-$, reacted with S341C when each was applied from the extracelluar side. Taken together, the results of Fatehi and Linsdell[37] and El Hiani and Linsdell[36] suggest that cysteines at positions 338 and 341 can be modified by $MTSET^+$ and $MTSES^-$ from either the extracellular side or the cytoplasmic side of the channel. The simplest interpretation of this overlapping reactivity would seem to be that the mixed disulfides can traverse the narrowest region of the pore, defined here as lying between positions 338 and 341. This result is especially surprising for $MTSET^+$ in view of the well-documented anion selectivity of CFTR.

The differences in the scanning results described above could, in principle, reflect some difference in protein conformation caused by the use of different cells or some other experimental condition such as the use of pyrophosphate to maximize channel open probability. Recently, however, we used temperature increases from 22 to 37 °C to effect substantial changes in the conformation of the outer vestibule of the CFTR pore that were evident from markedly increased rates of reaction of $MTSES^-$ with cysteines substituted at positions 334 and 336–338 at 37 °C.[62] In the case of F337C CFTR, a cysteine that was unreactive toward externally applied $MTSES^-$ at 22 °C was highly reactive at 37 °C. Despite these substantial changes in conformation, however, the position of the size selectivity barrier was unchanged. That is, even at 37 °C, a cysteine substituted at position 341 remained unreactive toward externally applied $MTSES^-$.

R352–D993 Salt Bridge. The CFTR molecular model and additional MD simulation presented here confirm the suggestion of the initial, more limited simulation[6] that R352 (TM6) and D993 (TM9) will periodically form a salt bridge that extends across the anion conduction path. Cui et al.[11] first proposed that these two residues might transiently form a salt bridge during the gating cycle of CFTR. On the basis of single- and double-charge changes, they suggested that the formation of the salt bridge stabilized the full, open state of the channel, whereas in its absence, anion conduction was dominated by lower conductance substates. Subsequently, Bai et al.[35] studied the effects of covalent modification of a cysteine at position 352 using inside-out patches detached from CHO cells. They found that R352C CFTR exhibited unstable gating and reduced current excursions reminiscent of the subconductance states reported by Cui et al.[11] Modification of R352C CFTR by either $MTSET^+$ or $MTSEA^+$ restored the full conductance state and appeared to stabilize the gating pattern. The molecular model and MD simulation presented here strongly support a scenario in which the formation of the R352–D993 salt bridge stabilizes the full open state of the CFTR pore by reducing the extents of relative motion of TM6 and TM9. The impact of salt bridge formation on anion conduction is difficult to predict quantitatively. Formation of the salt bridge is expected to alter the local electric field and perhaps to partially obstruct the conduction path (Figure 10).

Where Is the CFTR Gate? The template for the homology model of CFTR explored here and previously by Alexander et al.[6] was the crystal structure of Sav1866, an ABC transporter protein that carries out the energy-dependent export of drugs and antibiotics from bacterial cells.[24] A significant overall structural similarity between CFTR and Sav1866 is evident in the relative success of the Sav-based homology model in predicting experimentally demonstrable features of the CFTR anion conduction pathway, but any interpretation of the homology model must recognize a fundamental difference in the function of the two proteins. Sav1866 and virtually all its family members transport solutes by means of an alternating access mechanism that requires two gates, only one of which can be open at any one time.[65] This mechanism precludes ion conduction, that is, the rapid movement of ions driven by an electrochemical gradient, such as seen in the CFTR channel. CFTR is, so far, unique among the ABC transporter family in its ability to mediate ion conduction, a fact that has given rise to its being described as a "broken" or "degraded" transporter.[3,9] The crystal structure of Sav1866 captured the protein in its outward-facing conformation, that is, with the cytoplasmic gate closed and the nucleotide binding domains tightly dimerized, the latter condition being associated with the conducting state of the CFTR channel.[1,3] Not surprisingly, therefore, the Sav-based model of CFTR does not reveal the connection between the internal cavity and the cytoplasm that would be required for a truly "open," anion-conducting channel. Recent studies from two laboratories, in fact, suggest that a fundamental difference

in the CFTR protein may be the lack of any barrier to anion movement at the most cytoplasmic extent of the pore.[9,10] In both studies, cysteines engineered at positions in TM12 predicted to line the large internal cavity identified in our Sav-based model (e.g. 1141 and 1142) could be labeled by thiol-directed reagents applied to the cytoplasmic side of detached membrane patches even when the channels were bathed by solutions lacking ATP so that they were in a non-conducting conformation.[9,10] Thus, even in a "closed" CFTR channel the internal cavity is readily accessible from the cytoplasmic side of the pore. These results leave little doubt that whatever gate determines the conducting state of the CFTR channel, it cannot be located at the most cytoplasmic end of the pore defined by the Sav-based model. The results of Bai et al.,[9] however, are consistent with a narrowing of the cytoplasmic opening of the CFTR pore in the conducting conformation of the channel that may be reminiscent of the outward-facing conformation of Sav1866. They showed that for a rather large probe, MTSEA-Texas Red, the rate of reaction from the cytoplasmic side for cysteines at positions 1141 and 1148 in TM12 and 344 and 348 in TM6 was actually much greater when the channels were in a non-conducting state than when they were in a conducting state. Qian et al.[10] interpreted their results as providing evidence of a gate that lies deeper in the pore from the cytoplasmic side, near M1140 in TM12, although there are striking differences between their findings and those of Bai et al.[9] that are not easily resolved in terms of differences in experimental conditions. Rosenberg et al.[66] interpreted the results of electron diffraction by two-dimensional crystals of CFTR as suggesting a gate roughly at the level of R352 in TM6, but they also indicate that this could be an artifact produced by detergent bound within the crystals, an interpretation consistent with our Sav-based model. It seems unlikely, therefore, that the CFTR gate lies at the most cytoplasmic extent of the transmembrane segments. Further study will be required to determine if the pore bottleneck, which varies in diameter during the MD simulation, plays any role in channel gating.

Outer Vestibule Electrostatics. The Sav-based molecular model places R334 in the outer vestibule of the pore. Smith et al.[13] concluded that R334 made an important contribution to the electrostatic potential in the outer vestibule of CFTR. Eliminating this charge reduces the single-channel conductance and alters the shape of macroscopic and single-channel $I-V$ curves in the manner predicted by a charged vestibule model,[13,40] and subsequent studies have confirmed the impact of changes in charge at position 334 on conductance and the shape of the $I-V$ plot.[33,39] According to the charged vestibule model, the effect of eliminating R334 primarily attributable to a decrease in the local concentration of Cl^- at the outer rim of the bottleneck. This effect would tend to decrease the time-average concentration of Cl^- in the bottleneck, thereby reducing conductance.[52] The impact of the charge at position 334 on the apparent pK_a of a cysteine substituted at position 338[40] implies that the electrostatic field due to R334 is, indeed, sensed at the outermost rim of the pore bottleneck. Neutralizing the charge at position 334 shifts the apparent pK_a of a cysteine at position 338 by ~1 pH unit in the alkaline direction. Similarly, while both extracellular $MTSET^+$ and $MTSES^-$ react with a cysteine at position 338, the ratio of the rates of reaction (k_{MTSET^+}/k_{MTSES^-}) of these oppositely charged reagents was <1.0 for T338C/wt CFTR and >1.0 for T338C/R334D CFTR as expected if the charge at this position makes a major contribution to the electrostatic potential at the outer rim of the bottleneck.[40] Studies of the impact of covalent and noncovalent modifications at position 338 also argue that the electrostatic potential at this site, just on the outward-facing lip of the bottleneck, is critical for anion conduction. Simply increasing the partial negative charge on the cysteine thiolate anion engineered at position 338 by alkalinizing the pH of the external bath is sufficient to virtually abolish anion conduction.[40]

CONCLUSION

The results presented here suggest that the Sav1866-based homology model of the CFTR channel, while not perfect, is a significant step along the path to a molecular model that will be useful for understanding the nature of the anion conduction process and for in silico screening of potential CFTR modulators. Comparison of cysteine scanning results with the predictions of three homology models indicates that MD simulation will be a useful tool for exploring the conformational space accessible to the protein.

ASSOCIATED CONTENT

Supporting Information

Cross sectional areas of the CFTR pore along the pore axis (Figure S1), experimental results of a cysteine scan of TM3, TM6, TM9, and TM12 obtained using externally applied, channel-permeant and channel-impermeant reagents (Figure S2), cysteine scanning experiments at two residues in TM12 (Figure S3), and locations and distances of cysteine pairs employed in cross-linking experiments by Chen et al.[41] (Figure S4). This material is available free of charge via the Internet at http://pubs.acs.org.

AUTHOR INFORMATION

Corresponding Author

*Address: 3181 SW Sam Jackson Park Rd., L334, Portland, OR 97239. Phone: (503) 494-8738. Fax: (503) 494-4352. E-mail: norimats@ohsu.edu.

Author Contributions

Y.N., A.I., and C.A. made equal contributions to this work. The Dawson and Sansom laboratories made equal contributions to this work.

Funding

This work was supported by National Institute of Diabetes and Digestive and Kidney Diseases Grant DK45880 to D.C.D. and Cystic Fibrosis Foundation Grant DAWSON08G0 to D.C.D. M.S.P.S.'s laboratory was supported by the Wellcome Trust and the BBSRC.

Notes

The authors declare no competing financial interest.

ACKNOWLEDGMENTS

We are grateful to David Gadsby, T. C. Hwang, and the three reviewers for constructive comments on the manuscript. We also thank Frank Chen, Carly Chambers, Gregory Jungwirth, Daniel Nachreiner, and John MacDougall for their help in the laboratory.

ABBREVIATIONS

CFTR, cystic fibrosis transmembrane conductance regulator; ABC, ATP binding cassette; TM, transmembrane segment;

MD, molecular dynamics; $[Au(CN)_2]^-$, dicyanoaurate(I); $[Ag(CN)_2]^-$, dicyanoargentate(I); $MTSET^+$, [2-(trimethylammonium)ethyl]methanethiosulfonate; $MTSES^-$, (2-sulfonatoethyl)methanethiosulfonate; wt, wild type; 2-ME, 2-mercaptoethanol; DTT, dithiothreitol; KCN, potassium cyanide; rmsd, root-mean-square deviation; IBMX, 3-isobutyl-1-methylxanthine; DMPC, dimyristoylphosphatidylcholine; MSD, membrane-spanning domain; DPC, diphenylamine-2-carboxylate; CHO, Chinese hamster ovary; BHK, baby hamster kidney.

REFERENCES

(1) Gadsby, D. C., Vergani, P., and Csanady, L. (2006) The ABC protein turned chloride channel whose failure causes cystic fibrosis. *Nature 440*, 477−483.

(2) Hwang, T. C., and Sheppard, D. N. (2009) Gating of the CFTR Cl^- channel by ATP-driven nucleotide-binding domain dimerisation. *J. Physiol. 587*, 2151−2161.

(3) Chen, T. Y., and Hwang, T. C. (2008) CLC-0 and CFTR: Chloride channels evolved from transporters. *Physiol. Rev. 88*, 351−387.

(4) Mornon, J. P., Lehn, P., and Callebaut, I. (2008) Atomic model of human cystic fibrosis transmembrane conductance regulator: Membrane-spanning domains and coupling interfaces. *Cell. Mol. Life Sci. 65*, 2594−2612.

(5) Serohijos, A. W., Hegedus, T., Aleksandrov, A. A., He, L., Cui, L., Dokholyan, N. V., and Riordan, J. R. (2008) Phenylalanine-508 mediates a cytoplasmic-membrane domain contact in the CFTR 3D structure crucial to assembly and channel function. *Proc. Natl. Acad. Sci. U.S.A. 105*, 3256−3261.

(6) Alexander, C., Ivetac, A., Liu, X., Norimatsu, Y., Serrano, J. R., Landstrom, A., Sansom, M., and Dawson, D. C. (2009) Cystic fibrosis transmembrane conductance regulator: Using differential reactivity toward channel-permeant and channel-impermeant thiol-reactive probes to test a molecular model for the pore. *Biochemistry 48*, 10078−10088.

(7) Smith, S. S., Steinle, E. D., Meyerhoff, M. E., and Dawson, D. C. (1999) Cystic fibrosis transmembrane conductance regulator. Physical basis for lyotropic anion selectivity patterns. *J. Gen. Physiol. 114*, 799−818.

(8) Serrano, J. R., Liu, X., Borg, E. R., Alexander, C. S., Shaw, C. F. III, and Dawson, D. C. (2006) CFTR: Ligand Exchange between a Permeant Anion ($[Au(CN)_2]^-$) and an Engineered Cysteine (T338C) Blocks the Pore. *Biophys. J. 91*, 1737−1748.

(9) Bai, Y., Li, M., and Hwang, T. C. (2011) Structural basis for the channel function of a degraded ABC transporter, CFTR (ABCC7). *J. Gen. Physiol. 138*, 495−507.

(10) Qian, F., El Hiani, Y., and Linsdell, P. (2011) Functional arrangement of the 12th transmembrane region in the CFTR chloride channel pore based on functional investigation of a cysteine-less CFTR variant. *Pfluegers Arch. 462*, 559−571.

(11) Cui, G., Zhang, Z., O'Brien, A., Song, B., and McCarty, N. (2008) Mutations at arginine 352 alter the pore architecture of CFTR. *J. Membr. Biol. 222*, 91−106.

(12) Liu, X., Smith, S. S., Sun, F., and Dawson, D. C. (2001) CFTR. Covalent modification of cysteine-substituted channels expressed in *Xenopus* oocytes shows that activation is due to the opening of channels resident in the plasma membrane. *J. Gen. Physiol. 118*, 433−446.

(13) Smith, S. S., Liu, X., Zhang, Z. R., Sun, F., Kriewall, T. E., McCarty, N. A., and Dawson, D. C. (2001) CFTR. Covalent and noncovalent modification suggests a role for fixed charges in anion conduction. *J. Gen. Physiol. 118*, 407−432.

(14) Mense, M., Vergani, P., White, D. M., Altberg, G., Nairn, A. C., and Gadsby, D. C. (2006) In vivo phosphorylation of CFTR promotes formation of a nucleotide-binding domain heterodimer. *EMBO J. 25*, 4728−4739.

(15) Li, M. S., Demsey, A. F., Qi, J., and Linsdell, P. (2009) Cysteine-independent inhibition of the CFTR chloride channel by the cysteine-reactive reagent sodium (2-sulphonatoethyl) methanethiosulphonate. *Br. J. Pharmacol. 157*, 1065−1071.

(16) Holstead, R. G., Li, M. S., and Linsdell, P. (2011) Functional differences in pore properties between wild-type and cysteine-less forms of the CFTR chloride channel. *J. Membr. Biol. 243*, 15−23.

(17) Liu, X., Alexander, C., Serrano, J., Borg, E., and Dawson, D. C. (2006) Variable reactivity of an engineered cysteine at position 338 in cystic fibrosis transmembrane conductance regulator reflects different chemical states of the thiol. *J. Biol. Chem. 281*, 8275−8285.

(18) Pellegrini-Calace, M., Maiwald, T., and Thornton, J. M. (2009) PoreWalker: A novel tool for the identification and characterization of channels in transmembrane proteins from their three-dimensional structure. *PLoS Comput. Biol. 5*, e1000440.

(19) Ho, B. K., and Gruswitz, F. (2008) HOLLOW: Generating accurate representations of channel and interior surfaces in molecular structures. *BMC Struct. Biol. 8*, 49.

(20) Smit, L. S., Wilkinson, D. J., Mansoura, M. K., Collins, F. S., and Dawson, D. C. (1993) Functional roles of the nucleotide-binding folds in the activation of the cystic fibrosis transmembrane conductance regulator. *Proc. Natl. Acad. Sci. U.S.A. 90*, 9963−9967.

(21) Wilkinson, D. J., Mansoura, M. K., Watson, P. Y., Smit, L. S., Collins, F. S., and Dawson, D. C. (1996) CFTR: The nucleotide binding folds regulate the accessibility and stability of the activated state. *J. Gen. Physiol. 107*, 103−119.

(22) Mansoura, M. K., Smith, S. S., Choi, A. D., Richards, N. W., Strong, T. V., Drumm, M. L., Collins, F. S., and Dawson, D. C. (1998) CFTR: Anion binding as a probe of the pore. *Biophys. J. 74*, 1320−1332.

(23) Riordan, J. R., Rommens, J. M., Kerem, B., Alon, N., Rozmahel, R., Grzelczak, Z., Zielenski, J., Lok, S., Plavsic, N., Chou, J. L., Drumm, M., Iannuzzi, M. C., and Collins, F. S. (1989) Identification of the cystic fibrosis gene: Cloning and characterization of complementary DNA. *Science 245*, 1066−1073.

(24) Dawson, R. J., and Locher, K. P. (2006) Structure of a bacterial multidrug ABC transporter. *Nature 443*, 180−185.

(25) Dawson, R. J., and Locher, K. P. (2007) Structure of the multidrug ABC transporter Sav1866 from *Staphylococcus aureus* in complex with AMP-PNP. *FEBS Lett. 581*, 935−938.

(26) Hwang, T. C., and Sheppard, D. N. (1999) Molecular pharmacology of the CFTR Cl^- channel. *Trends Pharmacol. Sci. 20*, 448−453.

(27) Sheppard, D. N., and Welsh, M. J. (1999) Structure and function of the CFTR chloride channel. *Physiol. Rev. 79*, S23−S45.

(28) Anderson, M. P., Gregory, R. J., Thompson, S., Souza, D. W., Paul, S., Mulligan, R. C., Smith, A. E., and Welsh, M. J. (1991) Demonstration that CFTR is a chloride channel by alteration of its anion selectivity. *Science 253*, 202−205.

(29) Tabcharani, J. A., Linsdell, P., and Hanrahan, J. W. (1997) Halide permeation in wild-type and mutant cystic fibrosis transmembrane conductance regulator chloride channels. *J. Gen. Physiol. 110*, 341−354.

(30) Linsdell, P., Zheng, S. X., and Hanrahan, J. W. (1998) Non-pore lining amino acid side chains influence anion selectivity of the human CFTR Cl^- channel expressed in mammalian cell lines. *J. Physiol. 512*, 1−16.

(31) Illek, B., Tam, A. W., Fischer, H., and Machen, T. E. (1999) Anion selectivity of apical membrane conductance of Calu 3 human airway epithelium. *Pfluegers Arch. 437*, 812−822.

(32) Hasegawa, H., Skach, W., Baker, O., Calayag, M. C., Lingappa, V., and Verkman, A. S. (1992) A multifunctional aqueous channel formed by CFTR. *Science 258*, 1477−1479.

(33) Zhang, Z. R., Song, B., and McCarty, N. A. (2005) State-dependent chemical reactivity of an engineered cysteine reveals conformational changes in the outer vestibule of the cystic fibrosis transmembrane conductance regulator. *J. Biol. Chem. 280*, 41997−42003.

(34) Cymes, G. D., and Grosman, C. (2011) Tunable pKa values and the basis of opposite charge selectivities in nicotinic-type receptors. *Nature 474*, 526−530.
(35) Bai, Y., Li, M., and Hwang, T. C. (2010) Dual roles of the sixth transmembrane segment of the CFTR chloride channel in gating and permeation. *J. Gen. Physiol. 136*, 293−309.
(36) El Hiani, Y., and Linsdell, P. (2010) Changes in accessibility of cytoplasmic substances to the pore associated with activation of the cystic fibrosis transmembrane conductance regulator chloride channel. *J. Biol. Chem. 285*, 32126−32140.
(37) Fatehi, M., and Linsdell, P. (2008) State-dependent Access of Anions to the Cystic Fibrosis Transmembrane Conductance Regulator Chloride Channel Pore. *J. Biol. Chem. 283*, 6102−6109.
(38) Fatehi, M., and Linsdell, P. (2009) Novel residues lining the CFTR chloride channel pore identified by functional modification of introduced cysteines. *J. Membr. Biol. 228*, 151−164.
(39) Gong, X., and Linsdell, P. (2003) Molecular determinants and role of an anion binding site in the external mouth of the CFTR chloride channel pore. *J. Physiol. 549*, 387−397.
(40) Liu, X., Zhang, Z. R., Fuller, M. D., Billingsley, J., McCarty, N. A., and Dawson, D. C. (2004) CFTR: A Cysteine at Position 338 in TM6 Senses a Positive Electrostatic Potential in the Pore. *Biophys. J. 87*, 3826−3841.
(41) Chen, E. Y., Bartlett, M. C., Loo, T. W., and Clarke, D. M. (2004) The ΔF508 mutation disrupts packing of the transmembrane segments of the cystic fibrosis transmembrane conductance regulator. *J. Biol. Chem. 279*, 39620−39627.
(42) Ward, A., Reyes, C. L., Yu, J., Roth, C. B., and Chang, G. (2007) Flexibility in the ABC transporter MsbA: Alternating access with a twist. *Proc. Natl. Acad. Sci. U.S.A. 104*, 19005−19010.
(43) Aller, S. G., Yu, J., Ward, A., Weng, Y., Chittaboina, S., Zhuo, R., Harrell, P. M., Trinh, Y. T., Zhang, Q., Urbatsch, I. L., and Chang, G. (2009) Structure of P-glycoprotein reveals a molecular basis for poly-specific drug binding. *Science 323*, 1718−1722.
(44) Mornon, J. P., Lehn, P., and Callebaut, I. (2009) Molecular models of the open and closed states of the whole human CFTR protein. *Cell. Mol. Life Sci. 66*, 3469−3486.
(45) Liu, X., Smith, S. S., and Dawson, D. C. (2003) CFTR: What's it like inside the pore? *J. Exp. Zool., Part A 300*, 69−75.
(46) Tabcharani, J. A., Rommens, J. M., Hou, Y. X., Chang, X. B., Tsui, L. C., Riordan, J. R., and Hanrahan, J. W. (1993) Multi-ion pore behaviour in the CFTR chloride channel. *Nature 366*, 79−82.
(47) Linsdell, P., Tabcharani, J. A., and Hanrahan, J. W. (1997) Multi-ion mechanism for ion permeation and block in the cystic fibrosis transmembrane conductance regulator chloride channel. *J. Gen. Physiol. 110*, 365−377.
(48) Linsdell, P. (2001) Thiocyanate as a probe of the cystic fibrosis transmembrane conductance regulator chloride channel pore. *Can. J. Physiol. Pharmacol. 79*, 573−579.
(49) Fatehi, M., St Aubin, C. N., and Linsdell, P. (2007) On the origin of asymmetric interactions between permeant anions and the cystic fibrosis transmembrane conductance regulator chloride channel pore. *Biophys. J. 92*, 1241−1253.
(50) Linsdell, P. (2005) Location of a common inhibitor binding site in the cytoplasmic vestibule of the cystic fibrosis transmembrane conductance regulator chloride channel pore. *J. Biol. Chem. 280*, 8945−8950.
(51) Zhou, J. J., Li, M. S., Qi, J., and Linsdell, P. (2010) Regulation of conductance by the number of fixed positive charges in the intracellular vestibule of the CFTR chloride channel pore. *J. Gen. Physiol. 135*, 229−245.
(52) Dawson, D. C., Liu, X., Zhang, Z.-R., and McCarty, N. A. (2003) Anion Conduction by CFTR: Mechanisms and Models. In *CFTR Chloride Channel* (Kirk, K., and Dawson, D., Eds.) pp 1−34, Landes Bioscience, Georgetown, TX.
(53) Bockris, J. O. M., and Reddy, A. K. N. (1970) *Modern Electrochemistry*, Plenum Press, New York.
(54) Marcus, Y. (1994) A simple empirical model describing the thermodynamics of hydration of ions of widely varying charges, sizes, and shapes. *Biophys. Chem. 51*, 111−127.
(55) Marcus, Y. (1997) *Ion properties*, Marcel Dekker, New York.
(56) Kolbe, M., Besir, H., Essen, L. O., and Oesterhelt, D. (2000) Structure of the light-driven chloride pump halorhodopsin at 1.8 Å resolution. *Science 288*, 1390−1396.
(57) Ko, Y. J., and Jo, W. H. (2010) Chloride ion conduction without water coordination in the pore of ClC protein. *J. Comput. Chem. 31*, 603−611.
(58) Anslyn, E. V., and Dougherty, D. A. (2005) *Modern Physical Organic Chemistry*, University Science Books, Sausalito, CA.
(59) McDonough, S., Davidson, N., Lester, H. A., and McCarty, N. A. (1994) Novel pore-lining residues in CFTR that govern permeation and open-channel block. *Neuron 13*, 623−634.
(60) Linsdell, P. (2001) Relationship between anion binding and anion permeability revealed by mutagenesis within the cystic fibrosis transmembrane conductance regulator chloride channel pore. *J. Physiol. 531*, 51−66.
(61) McCarty, N. A., and Zhang, Z. R. (2001) Identification of a region of strong discrimination in the pore of CFTR. *Am. J. Physiol. 281*, L852−L867.
(62) Liu, X., and Dawson, D. C. (2011) Cystic fibrosis transmembrane conductance regulator: Temperature-dependent cysteine reactivity suggests different stable conformers of the conduction pathway. *Biochemistry 50*, 10311−10317.
(63) Linsdell, P., and Hanrahan, J. W. (1996) Disulphonic stilbene block of cystic fibrosis transmembrane conductance regulator Cl^- channels expressed in a mammalian cell line and its regulation by a critical pore residue. *J. Physiol. 496*, 687−693.
(64) Linsdell, P., Tabcharani, J. A., Rommens, J. M., Hou, Y.-X., Chang, X.-B., Tsui, L.-C., Riordan, J. R., and Hanrahan, J. W. (1997) Permeability of wild-type and mutant cystic fibrosis transmembrane conductance regulator chloride channels to polyatomic anions. *J. Gen. Physiol. 110*, 355−364.
(65) Gadsby, D. C. (2009) Ion channels versus ion pumps: The principal difference, in principle. *Nat. Rev. Mol. Cell Biol. 10*, 344−352.
(66) Rosenberg, M. F., O'Ryan, L. P., Hughes, G., Zhao, Z., Aleksandrov, L. A., Riordan, J. R., and Ford, R. C. (2011) The cystic fibrosis transmembrane conductance regulator (CFTR): Three-dimensional structure and localization of a channel gate. *J. Biol. Chem. 286*, 42647−42654.